VISCOELASTIC SHEAR DAMPING MECHANISM FOR VIBRATION REDUCTION ON A HELICOPTER ANTI-TORQUE BEAM

Bottasso Luigi M.[1], Ghiringhelli Gianluca[2], Perazzolo Alessandro[1], Fosco Ermanno[1], Ricciardi Massimo[1], Goh Chee Su[1], Vigoni Edoardo[3], Cordisco Potito[3], Terraneo Mauro[3], and Vertel John[4]

[1]Leonardo Helicopters, [2]Politecnico di Milano, [3]VICOTER, [4]UTC Aerospace Systems

Abstract

We describe the design and test of improved versions of the anti-torque beam (ATB) of the AW139 twin-engine helicopter, featuring multi-layered viscoelastic damping treatment. Viscoelastic material sheets have been embedded in the component to damp vibrations over a wide frequency spectrum. The new configuration is called hybrid anti-torque beam (HATB). Two approaches have been pursued; in the first, a completely new multi-layer laminated beam was built, replacing the original monolithic structure with a sandwich of metal sheets interposed with viscoelastic material. Different sub-cases were explored and ground-tested. The second configuration, which is easier to qualify for flight test, was based on a standard production beam. The part was coated on both sides with a proprietary high-damping treatment, suitably constrained in order to activate a shear strain mode. The adoption of high-damping material in a structural component such as the ATB facilitates the dissipation of mechanical energy in transit through the part, before it is converted into acoustic energy. The location of the ATB is strategic in this respect because it represents a privileged transfer path for vibrations generated by the main rotor, transmission gearbox, engines, pumps, cooling fans and other utilities. A test campaign offered some experimental insight on those design factors which mostly affect the damping, aimed at achieving an optimal trade-off between structural stiffness, weight and loss factor. The preliminary flight and ground tests of the HATB have shown that it can be effective in attenuating the noise transmitted to the helicopter cabin. These results will enable further development and testing of multi-layer HATB designs.

1 INTRODUCTION

Despite the undeniable advances achieved in crew and passenger comfort on modern helicopters, the internal cabin noise remains a tough problem to tackle.

Achieving high levels of sound proofing requires careful consideration of several distinct aspects, including trim panel material selection and design, minimised leakage along the trim panel edges, optimised manufacturing processes and panel installation, damped trim panel attachments, window gaskets, carpets etc.

Most common noise abatement approaches are passive, even though some active noise cancellation systems are available. However, sound waves at the medium frequency range (1500-5000 Hz) are difficult to cancel in three dimensions due to their relatively short audio wavelength in air (7-23 cm).

In addition to acoustic liners, one can think of making structures which are intrinsically less prone to vibration by increasing their damping characteristics.

Traditionally, the design of aeronautical structures has focused on strength-to-weight, fatigue life and crashworthiness criteria, while addressing the acoustic impedance of structures has never been a priority. In this respect, modern composite structures have compounded the problem because they have even less structural damping than metal ones; the transmissibility of acoustic vibrations from the airframe to the cabin interior is thus increased[1].

The approach described in this paper is the use of materials having very high intrinsic damping, aimed at reducing the noise transmissivity of structures[2][3].

The anti-torque beam (ATB) is a structural element whose function is to transfer the torque of the main rotor from the transmission gearbox to the helicopter fuselage. Figure 1 illustrates the ATB location within the AW139 helicopter drivetrain assembly.

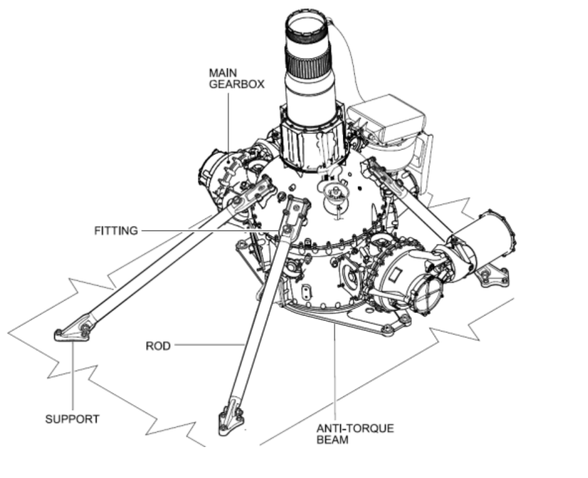

Figure 1: The anti-torque beam and main gearbox of the AW139

Figure 2 shows the overall shape of two anti-torque beam test articles.

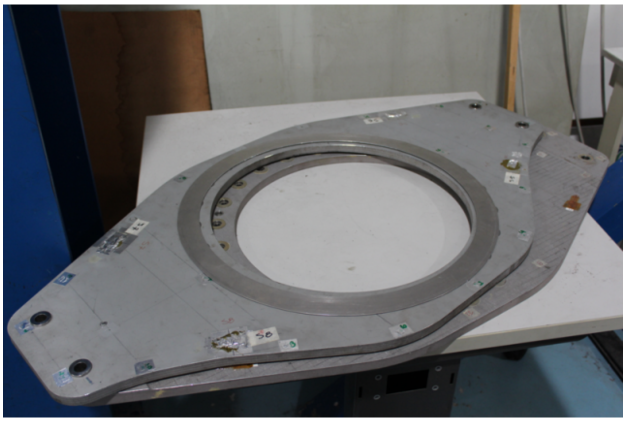

Figure 2: Anti-torque beam test articles

During operation, the ATB is mainly subjected to an in-plane torque through the main gearbox (MGB) onto which it is bolted. The rotor loads, mainly the aerodynamic forces and moments generated by the blades, are transferred to the airframe through four MGB support struts. However, significant in-plane reactions are applied to the ATB besides the torque, as well as a residual out-of-plane load component.

The ATB transfers vibration energy (up to 5 kHz) into the fuselage due to its location in close proximity of the gearbox drivetrain and the engines.

The typical spectrum of a helicopter cabin noise is a mix of broadband and tonal noise, the latter being generated at specific frequencies by intermeshing drivetrain gears as well as by the engines and the oil pumps (see Appendix, Figure 36).

The standard ATB part, which is essentially a monolithic plate of 7075-T6 aluminum alloy [4] [5] (σ_t 524 MPa, σ_y 462 MPa), does not allow for any vibration dissipation because the bare material has very small intrinsic damping. Furthermore the ATB is rigidly connected to the helicopter airframe through four bolted flange attachments, as illustrated in Figures 1 and 2.

We aimed at addressing the problem by studying and testing modified ATB designs which can provide high levels of damping over a broad frequency spectrum, including the acoustic range.

2 STRUCTURAL DAMPING DESIGN CONFIGURATIONS

The chosen approach consisted of a layered ATB structure with rubber sheets sandwiched between metal plates, and bonded to them, leading to a so-called hybrid ATB or HATB [6]; two specimens are pictured in Figure 2.

These are examples of the more general concept of laminated hybrid materials, where viscoelastic layers are interposed between structural layers (metal or composite) for mechanical energy dissipation. The concept is illustrated in Figure 3, while Figure 4 shows material coupons.

This approach to distributed damping shall be seen in contrast to the more common lumped application, where an elastomeric bearing is used in series with a load-carrying structure, thus operating under high stress level [7].

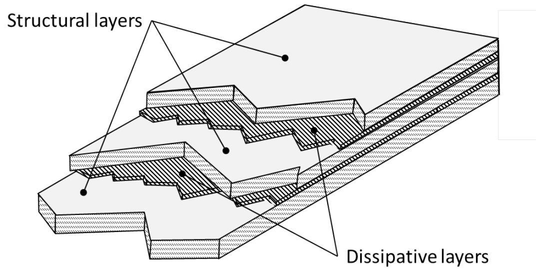

Figure 3: The structure of a hybrid laminated material

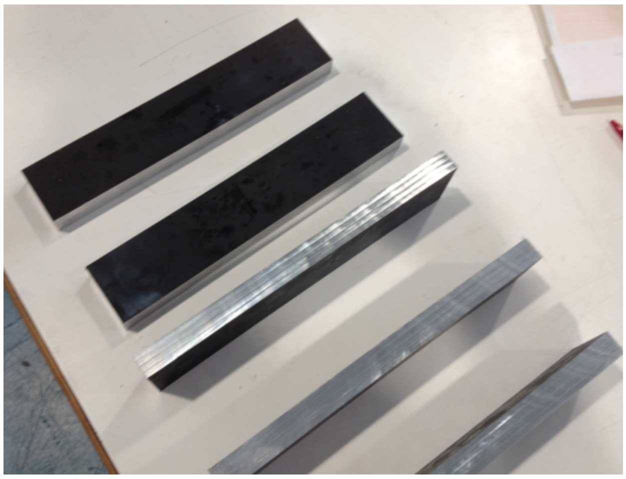

Figure 4: Hybrid laminated material test coupons

The use of a high intrinsic damping material allows for effective dissipation of mechanical energy while it is travelling through the component, before it is transformed into noise. This is possible thanks to the dissipative efficiency of relatively small amounts of viscoelastic material spread into the structure (see Appendix A.1).

Analytical studies backed by experiments have shown that good performances are achieved in a stack with metal plates having a thickness of a few mm with interposed viscoelastic sheets of a few tenths of mm.

The viscoelastic material has to be thin to avoid large strains and thus large deformations of the sandwich section. However, even a relatively small viscoelastic thickness is beneficial in damping vibrations through shear stress cycles and the associated hysteresis in the viscoelastic material.

Obviously, the multi-layer HATB configuration shall meet the same static strength requirements of the standard component.

The dissipative effect in the HATB sandwich at a given frequency is mainly related to the structure's capability to vibrate out-of-plane in bending mode at that frequency. When bending deflection is dominant during vibration the rubber layers transfer loads from one structural layer to the other through shear strain. This "series-mode" is the optimal condition for energy dissipation.

The interlaminar shear stress varies with a parabolic shape through the beam section thickness, reaching its maximum at the section neutral axis and zero at the top and bottom surfaces, as shown in Figure 5.

Thus the dissipative layers at or near the section midline will be the most effective in damping vibrations because they are the most strained.

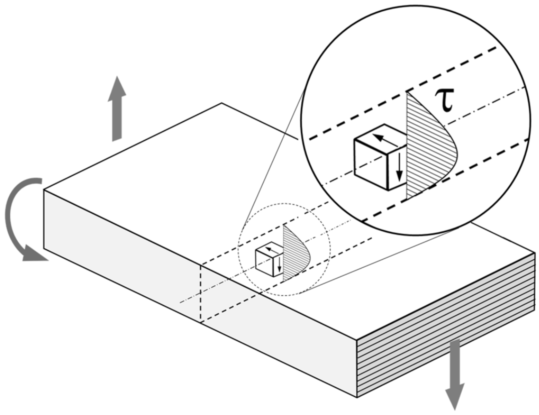

Figure 5: Shear stress profile through the thickness of a beam

Due to the above, the marginal benefits associated with additional viscoelastic layers tend to vanish, since the outer layers in the laminated material have decreasing damping effect.

On the contrary, when an in-plane (membrane) deformation mode is active, the layers in the sandwich panel work in parallel. During in-plane vibration most of the energy flows along the stiffer path, i.e. the structural (metal) layers, while the rubber is strained by continuity requirements.

In this condition the strain experienced by the viscoelastic material is very low, the associated hysteresis cycle is small and so is the energy dissipation.

As a consequence of the above, structural elements unable to activate shear strain modes will not benefit from the concept and will be ineffective in dissipating vibrational energy.

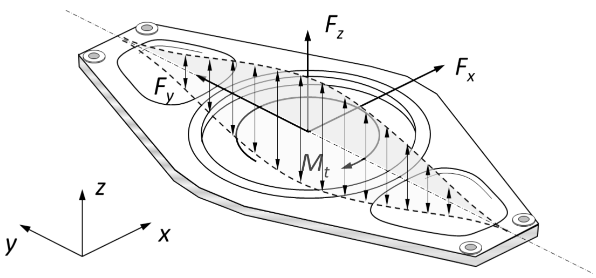

Figure 6: Loads acting on an anti-torque beam; the out of plane vibration mode (shaded) activates shear damping

The ATB shape, constraint system and loading from the MGB allow for the activation of bending modes, thus it is a component which lends itself well to a multi-layered configuration.

Figure 6 illustrates the loads transferred by the gearbox to the HATB, highlighting an example of the out-of-plane vibration mode which can benefit from a multi-layer construction.

The HATB viscoelastic treatment is mainly targeted at addressing z-direction modal shapes; these are excited not only by the vertical dynamic forcing, but also by the interactions of all components.

Each of the operational load components acting on the HATB is the combination of a relatively large static (or quasi-static) part and a dynamic part with wide frequency spectrum and small magnitude, responsible for vibrations.

The dominant (quasi) static operational load is the MGB torque M_t whose value can exceed 60 kNm. Furthermore, the HATB is subjected to significant in-plane forces which can reach up to 60 kN and 30 kN in x and y respectively, depending on the helicopter maneuver. There is also a residual out-of-plane load of much smaller magnitude.

2.1 HATB design

Two design approaches were pursued: in the first, completely new multi-layer laminated beams were designed and built, replacing the original monolithic structure with a sandwich of metal sheets interposed with viscoelastic material.

In order to ensure a high level of peeling strength in the metal-rubber bonding, natural (non vulcanized) rubber sheets were first glued to the aluminum plates and later cured in autoclave at around 6 bar and $160\,^{\circ}\mathrm{C}$ to attain extra bonding performance.

Different sub-cases were explored and ground tested, featuring different numbers of layers and thicknesses, using both synthetic styrene-butadiene rubber[8] (SBR) and neoprene (chloroprene), the latter adopted for its good weathering resistance. These are indicated in Table 1 as Types A, B and C.

The second configuration, easier to qualify for flight test, was based on a standard production beam and is indicated as Type D in Table 1. The part was coated on both sides with a damping treatment. The coating consisted of glass fiber reinforced panels with a proprietary viscoelastic matrix having a high loss factor. Aluminum closure sheets were bonded to the panels to allow proper shear activation of the elastomer under load.

Table 1: Different anti-torque beam types evaluated; Std refers to the current production design

Type	Composition (n. of layers x thickness)	
	7075-T6 alloy	Viscoelastic sheets
Std	13.5 mm monolithic	none
A	17 x 0.5 mm (1 mm for top and bottom plates)	18 x 0.33 mm SBR
B	4 x 3.85 mm	3 x 0.279 mm SBR
C	4 x 4 mm	3 x 0.44 mm chloroprene
D	Std ATB + 4.877 mm top plate and 0.813 mm bottom plate	2 x 3.175 mm glass fiber reinforced panels with proprietary elastomeric matrix

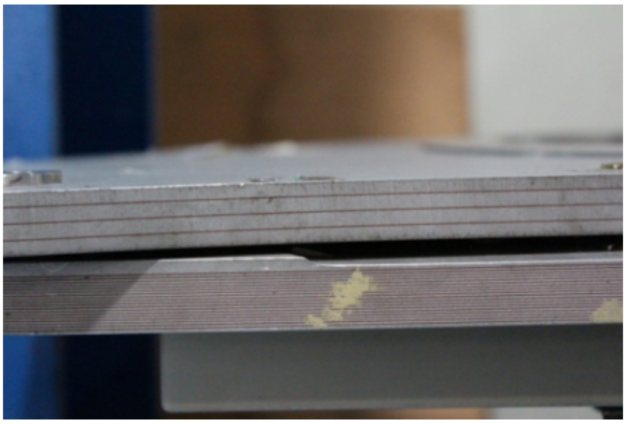

Figure 7: HATB Types A (bottom) and B

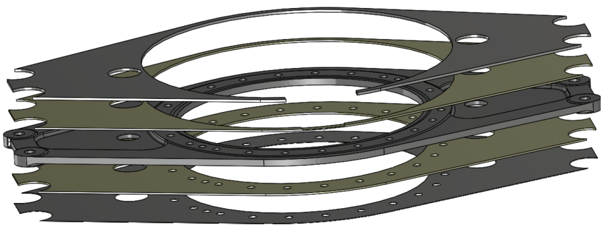

Figure 8: HATB Type D layer stacking

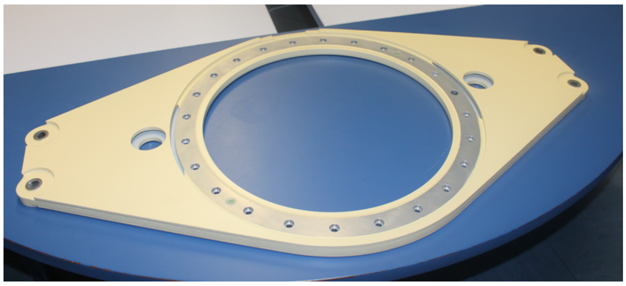

Figure 9: The completed HATB Type D

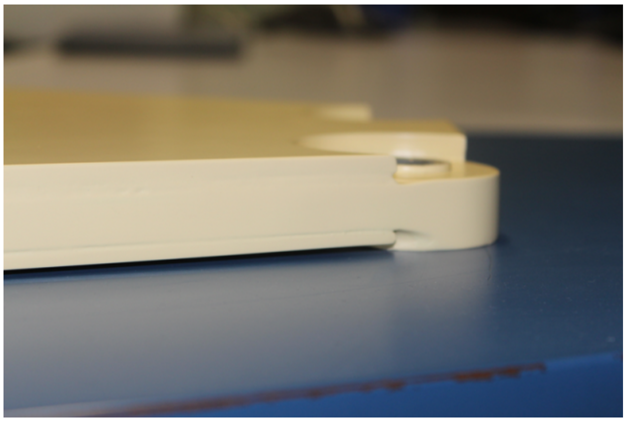

Figure 10: Close-up of the Type D layer stacks near the attachment flanges

3 HATB MODELLING AND TESTING

NASTRAN finite-element models for static, dynamic, linear and non-linear analyses were developed to model the full HATB as well as hybrid material test coupons to correlate experiments.

During the characterization of the new multi-layer laminates, models were used to numerically simulate 3-point bending tests of material coupons; these models included both geometric non-linearities (through NLPARM card) and material non-linearities through viscoelastic creep models of the form:

$$\varepsilon = \frac{\sigma}{E_0} + \frac{\sigma}{E_1}(1 - e^{-Rt}) \quad (1)$$

SBR elastomer material properties used in the FE models are presented in Table 2

Table 2: SBR rubber properties used in coupon FE models

Property	Symbol	Value	Units
Elastic Modulus (linear)	E_0	4.0-5.0	MPa
Elastic Modulus (creep)	E_0	6.2	MPa
Poisson's Modulus	ν	0.48	
Density	ρ	1463	kg/m^3
Creep coeff. a	$1/E_1$	2.2E-7	MPa^{-1}
Creep coeff. b	R	1.5E-2	s^{-1}

Static non-linear models were developed to predict buckling onset under extreme torque loading in the new multi-layer HATB design. The Type A HATB was found prone to buckling under static test and was therefore replaced by Types B and C which are stiffer and more stable due to the thicker metal plates.

Figures 11 and 12 illustrate the detailed FE model used for buckling prediction. Thanks to the correlation between the model and the buckling onset observed in the test of HATB Type A it was possible to evaluate the rubber elastic modulus in Table 2 with more precision.

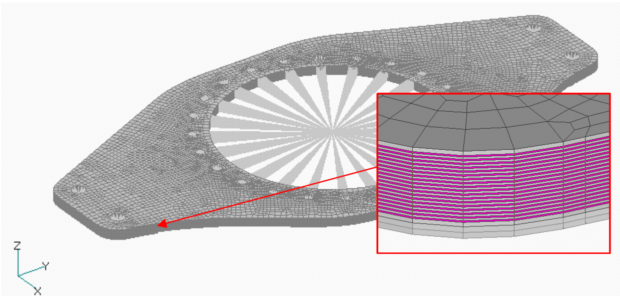

Figure 11: The static analysis FE model of the Type A HATB

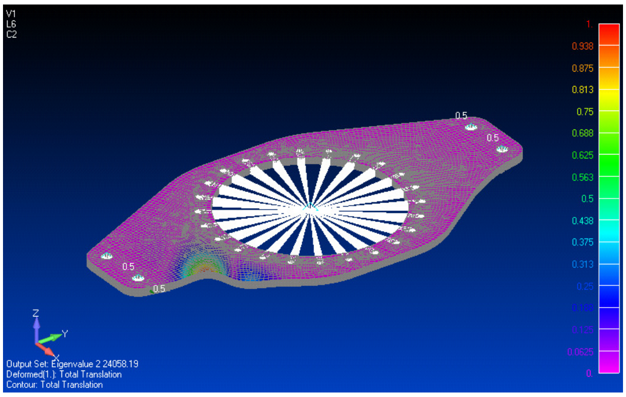

Figure 12: Buckling onset in the non-linear FE model of the Type A HATB

Dynamic models of the full HATB were built with NASTRAN PCOMP elements[9], a feature typically used for composite materials. Here the viscoelastic layers were not separately modelled, rather the mechanical properties of a virtual material were tailored to match the combined effect of metal and rubber for optimal correlation with the HATB dynamical test results; Figure 13 shows the dynamic analysis FE model.

The model could be used, among other things, to verify the suitability of the HATB in operation. By plugging the HATB in the global FE model of the helicopter it is possible to check that no structural resonances can be triggered by the new beam once it is installed on the real airframe.

To this purpose, the model PCOMP properties were tuned to achieve a good match with the eigenvectors and eigenmodes derived from rap-testing of the real beam (see Figure 16). The tuning resulted in rubber modulus properties deviating from the values in Table 2; this was partly due to certain dynamic model simplifications which could not account e.g. for frequency-dependent moduli E, G.

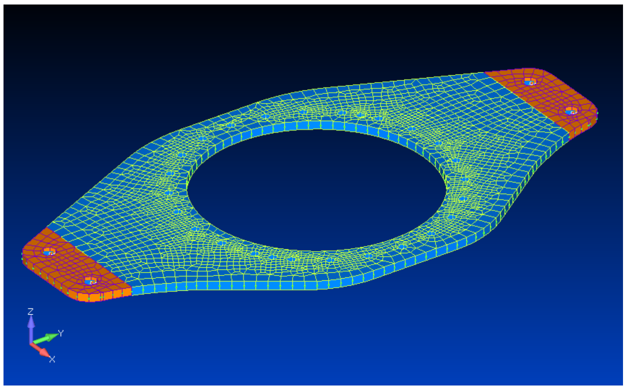

Figure 13: The dynamic FE model of the HATB

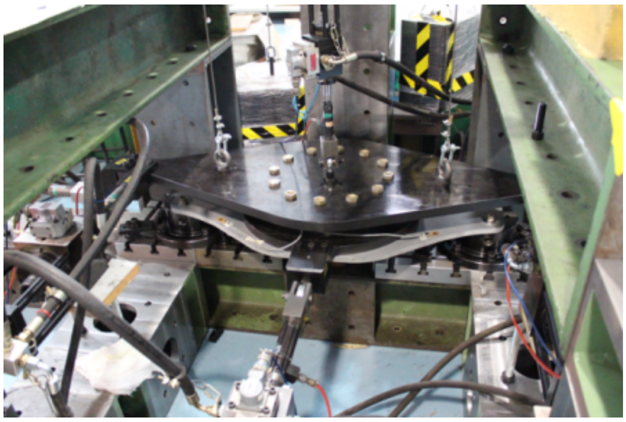

Figure 14: The HATB under test in the static / fatigue rig (the black plate is used to transfer the simulated MGB torque)

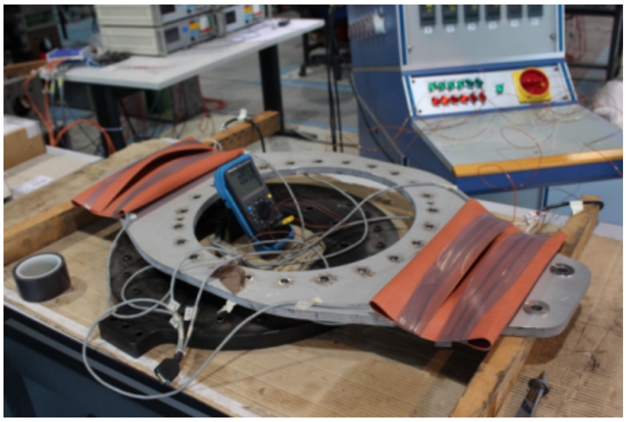

Figure 15: Type C HATB was fatigue-tested with thermal blankets to simulate operating conditions in close proximity of the MGB and the engines, where temperature can affect rubber properties

Static and fatigue tests were conducted on all multi-layer HATB prototypes to qualify the new material in view of future experimental flight demonstration. Figure 14 shows the beam on the rig under fatigue test at room-temperature.

Figure 15 illustrates the thermal blankets which were later added to verify the static/fatigue performance under more realistic thermal conditions in operation; in-fact, due to its proximity to the transmission drivetrain and the engines, the HATB can reach temperatures exceeding $70\,^{\circ}\mathrm{C}$ (though not in normal operating conditions), depending on OAT (outside air temperature) and flight phase.

3.1 Damping results from laboratory test

We carried out experimental tests for the acquisition of modal parameters of the different HATB demonstrators.

The acquisitions were performed in free-free mode obtained by hanging the structure through an elastic suspension realized by bungee cords and subjecting it to repeated rap tests[10] as shown in Figure 16.

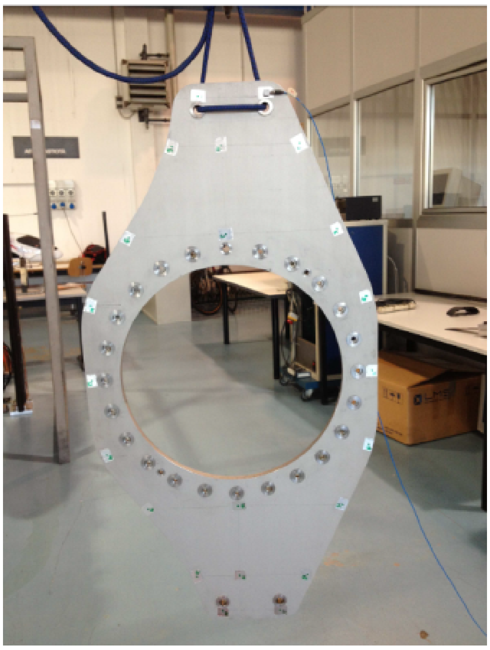

Figure 16: The HATB hanging on bungee lines prior to rap testing

The dynamic properties were derived through a roving impact hammer with force transducer on 22 separate locations; out-of-plane responses were measured by a uniaxial accelerometer placed in a fixed position.

The structure was excited only in the direction normal to its plane. The in-plane modes occur at much higher frequencies and for this reason they have not been investigated.

Two different test setups were considered for each HATB design; the first investigated the dynamic behavior of the bare plate, while in the second a very stiff steel ring was bolted onto the plate to simulate the gearbox.

Figures 17 and 18 display the sum of the acquired Frequency Response Functions in the two conditions analysed (as examples, only plate Types B and C are plotted).

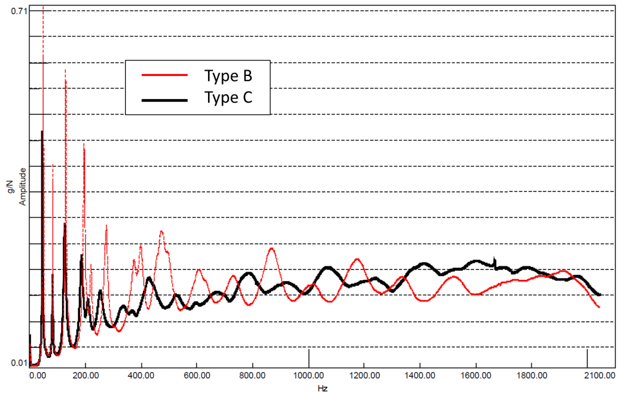

Figure 17: Comparison of the experimental FRF in free-free condition for the HATB Types B (red) and C (black) showing the improved damping performance of the chloroprene-based elastomer

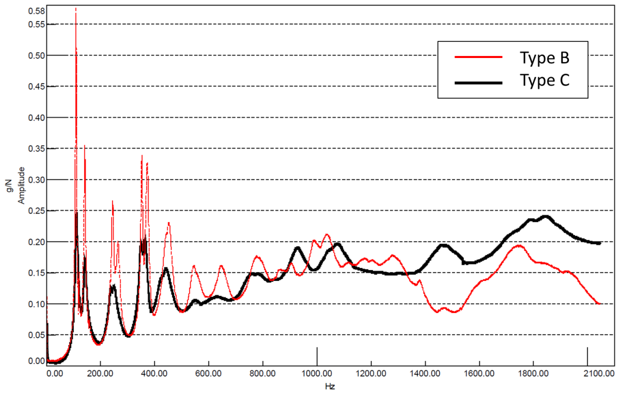

Figure 18: Comparison of the experimental FRF for the HATB Types B (red) and C (black) with MGB-simulator ring installed

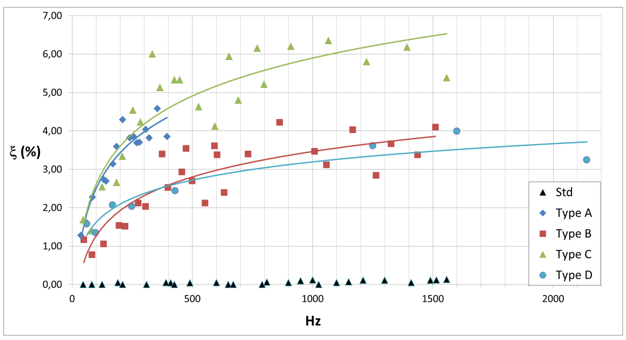

Figure 19: Comparison of critical damping for different HATB layering

The damping characteristics were assessed by measuring the vibration amplitude logarithmic decrement δ defined as

$$\delta = \frac{1}{r}\ln\left(\frac{x_i}{x_{i+r}}\right) = \frac{2\pi\xi}{\sqrt{1-\xi^2}} \tag{2}$$

and depicted in Figure 20

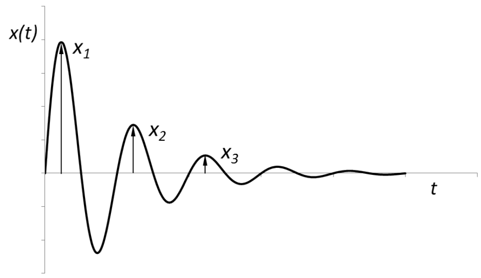

Figure 20: Transient response of underdamped SDOF system

The overall survey of the different HATB designs is summarised in Figure 19.

Figure 19 clearly shows the superior damping performance of the Type C HATB, which is better than Type A despite the much larger number of dissipative layers of the latter. This can be explained in part by the different material properties, and partially by the fact that only the layers closer to the plate mid-section contribute substantially to overall damping. In Types B and C HATBs one third of the whole viscoelastic material mass is concentrated in the optimal mid-section location.

The higher damping of Type C compared to B is explained both by the different material and also by the fact that the viscoelastic layers in Type C are almost 60% thicker, thus increasing the overall volume of dissipative material.

The relatively lower damping performance of the Type D is a function of its different HATB design, where the dissipative layers are located in a sub-optimal position, towards the upper and lower surfaces of the beam. This is because Type D was derived through a modification of a standard ATB.

3.2 Flight test campaign

A test campaign has been conducted, provisionally limited to the HATB Type D. In light of the critical structural relevance of the ATB, the effort required for the qualification and flight clearance of entirely new HATB designs such as Types A, B and C was considered more risky, and was therefore postponed to a future phase.

The Type D HATB instead, being essentially a standard production part with the addition of a damping treatment, lent itself to a much simpler flight clearance process.

The goal of the flight campaign was two-fold: to assess the acoustic impact of the HATB on internal cabin noise, and to verify the damping loss factor in terms of reduced structural vibration in proximity of the HATB connection points.

An AW139 twin-engine helicopter testbed was used for the flight campaign (Figure 21). The cabin configuration was bare with virtually no acoustic lining.

Figure 21: AW139 testbed

This fact had the consequence of introducing a substantial level of undesired background noise in the cabin, potentially making the detection of beneficial effects harder to measure.

The HATB tests were preceded by baseline flights with the standard production ATB installed on the helicopter.

The instrumentation consisted of twelve accelerometers and four microphones. Two triaxial accelerometers were placed on the gearbox and another six in close proximity to the beam's connection bolts, as illustrated in Figure 22.

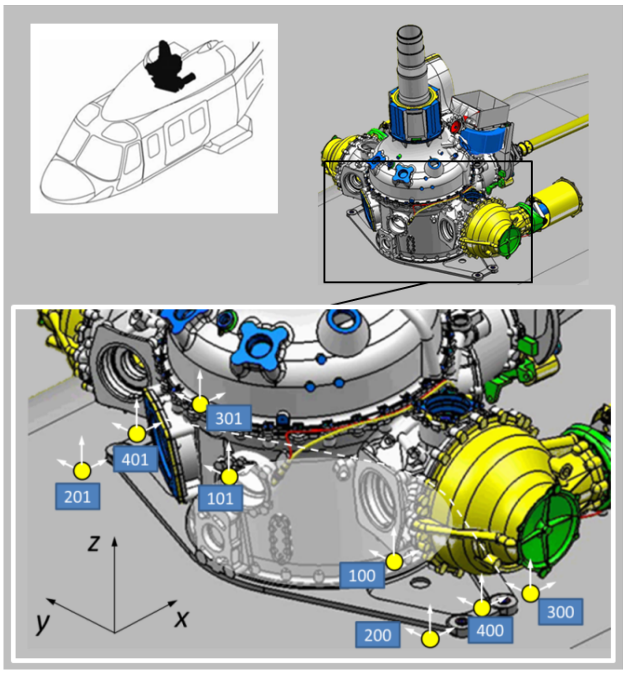

Figure 22: Position of accelerometers on ATB and MGB

Figures 23 and 24 show a close-up of the actual sensors installed in the MGB bay of the helicopter, respectively for the standard ATB and for the HATB. The remaining four accelerometers, uniaxial, were located on the roof structure inside the cabin.

The microphones were placed in points representative of the front and rear seat rows at the height of the passengers' heads, in a square configuration: front-left/right and rear-left/right. The helicopter used for the test was a prototype with an instrumentation rack installed in the middle of the cabin, as shown in Figure 25.

Figure 23: 3-axis accelerometers installed on RH side of standard ATB for baseline flight

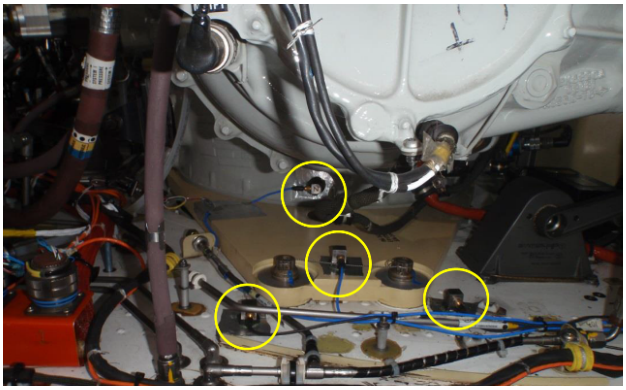

Figure 24: 3-axis accelerometers installed on LH side of Type D HATB

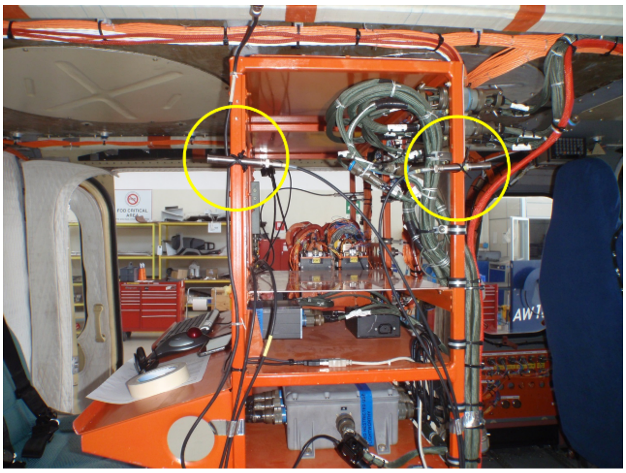

Figure 25: Microphone positions

Table 3 describes the different flight conditions during which the experimental data were collected.

Table 3: Flight conditions (HOGE: Hover Out of Ground Effect)

n.	IAS (kts)	Condition	Alt. (ft)
1	0	HOGE	
2	40	flight	3000
3	80	flight	3000
4	120	cruise	3000
5	140	cruise	3000
6	40	steep approach @ 500 fpm descent rate	

3.3 Experimental data from flight tests

Figure 26 summarizes vibration response data in a visually intuitive way, highlighting the vibration path from the MGB (points 100, 101) to the areas near the attachment bolts (points 200, 300, 400, 201, 301, 401). In this context it is more meaningful to show the acceleration gradient rather than its absolute values.

In particular the plots refer to vibrations at the main MGB frequency (f_{MGB}). This frequency, in the kHz range, is associated with gear meshing and is of particular interest because it represents the single most annoying source of tonal noise in the cabin.

Each plot shows an overlay of all flight conditions and compares the new HATB to the standard design, in terms of vertical (out of plane) acceleration. The vertical component, as expected, is the only one significantly affected by the viscoelastic damping of the HATB.

Results showed a tangible vertical vibration reduction through the HATB at the frequency of interest. The effect is distinctly visible also at other frequencies, though to a lower degree.

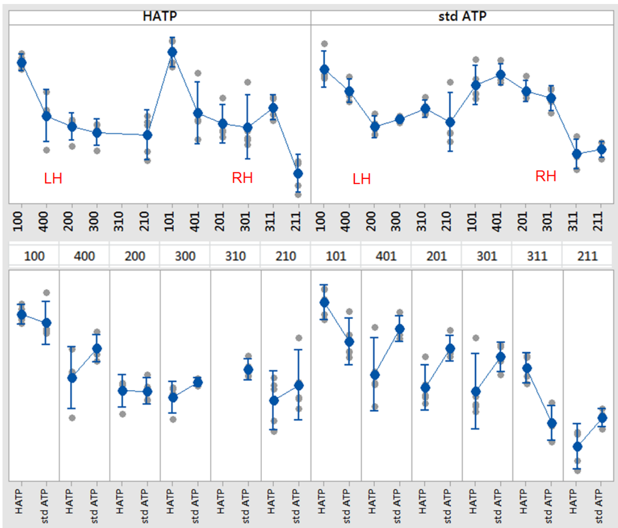

Figure 26: Vertical accelerations @ f_{MGB} - all flight conditions (LH and RH refer to the left and right sides of the MGB)

Points 210, 310, 211 and 311 represent the uniaxial accelerometers attached to the cabin roof panels; their responses were not very meaningful. Their position and relative distance from the vibration source rendered their responses not easily correlated to the level of acceleration at the HATB bolts.

Figures 27, 28, 29, 30, 31 and 32 illustrate the cabin noise spectra, average over the four microphones recorded for the six flight conditions of Table 3 (see also Appendix A.2).

It is noteworthy that for all flight conditions the HATB demonstrated a distinct noise benefit at and above the frequency of interest f_{MGB} which is the one at which peak SPL is reached, and which typically represents a particularly annoying pitch. The reduction in SPL, in the 7-10 dB(A) range, can be considered very significant (see Table 4).

The HATB, as expected, does not offer benefits at lower frequencies.

In terms of Speech Interference Level (SIL-4, see Appendix A.2) the benefits are not so dramatic; this is obvious since the SIL-4 is computed as the average over four octave bands which encompass frequencies which are not abated by the HATB. However, we observed a non-negligible reduction of around 2 dB, as shown in Table 5.

A summary of the key results both for SPL and SIL-4 is shown in Tables 4 and 5.

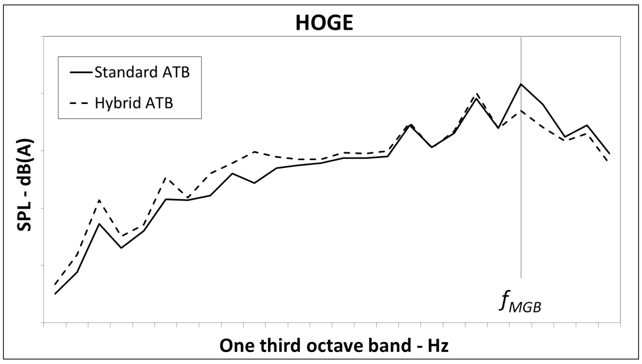

Figure 27: SPL comparison, flight condition: HOGE

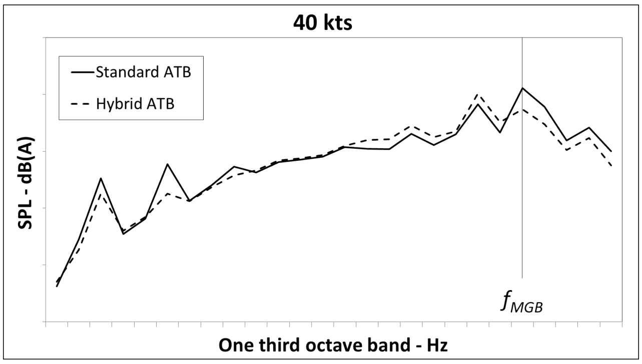

Figure 28: SPL comparison, flight condition: 40 kts

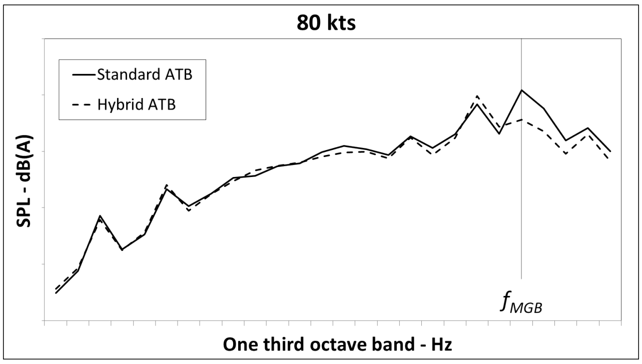

Figure 29: SPL comparison, flight condition: 80 kts

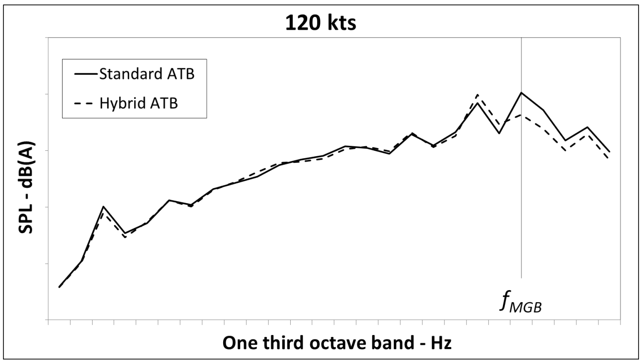

Figure 30: SPL comparison, flight condition: 120 kts

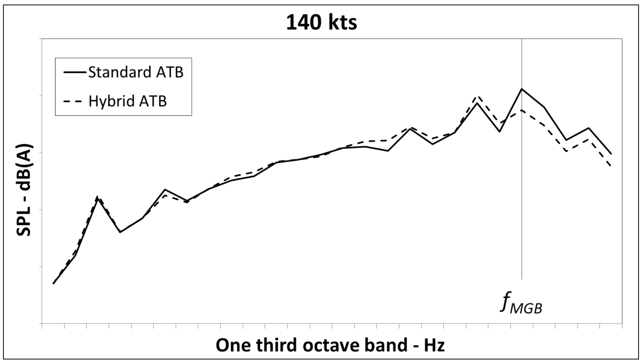

Figure 31: SPL comparison, flight condition: 140 kts

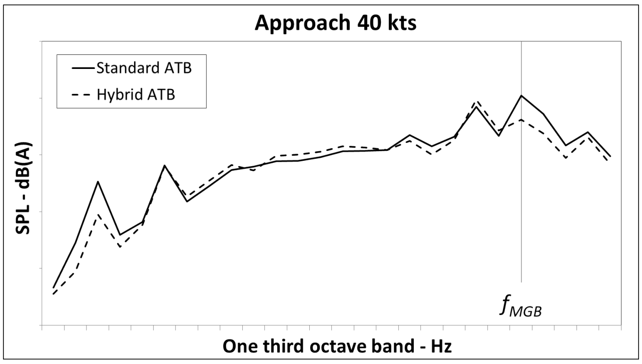

Figure 32: SPL comparison, flight condition: approach @40 kts

Table 4: Reduction of peak SPL @ MGB frequency

Condition	SPL reduction (dB(A))
HOGE	-9.3
40 kts	-8.3
80 kts	-10.4
120 kts	-7.8
140 kts	-7.4
approach	-8.4

Table 5: SIL-4 benefit

Condition	SIL-4 reduction (dB)
HOGE	-2.1
40 kts	-2.2
80 kts	-2.3
120 kts	-1.4
140 kts	-1.3
approach	-1.8

4 CONCLUSIONS AND NEXT STEPS

We have presented an overview of a research project aimed at evaluating a potential future application of laminated elastomeric-metal hybrid materials for vibration and noise reduction on helicopters.

These materials are effective in damping structural vibration over the acoustic spectrum and we observed that they can contribute to cabin noise reduction and thus improve acoustic comfort if properly integrated in the overall structural design.

The chosen application, the anti-torque beam, is a structural element which lends itself well to a hybrid design with improved damping. By its very nature, the ATB represents a preferred transit path for vibrations originating in the transmission drivetrain and proceeding towards the cabin structure resulting in noise within the cabin.

Hybrid materials could potentially represent a novel structural concept for more ambitious distributed applications, for example in cabin structural panels. Obviously the qualification process would not be easy, and should take into account critical factors such as the behaviour of rubber-like materials under fire exposure, aging etc. All these are beyond the scope of the present work.

During lab tests, the different HATB designs demonstrated varying levels of vibration damping capability over a wide frequency spectrum. For the HATB Type D, the flight test confirmed good vibration damping properties which translated into significant noise reduction inside the cabin.

It is of particular interest the fact that the HATB was able to abate the main SPL peak (occurring at the intermeshing frequency of the MGB) by 7-10 dB(A). This frequency is known to be especially annoying to cabin occupants.

The SIL-4, a measure of the ability to understand human conversation, improved only slightly (between 1.3 and 2.3 dB). The limited gain is a direct consequence of the fact that SIL-4 is computed over a broad frequency range extending four octaves, typical of human voice, thus only broad-frequency noise reduction measures can substantially improve it.

It shall also be noted that the most effective structural damping designs of the HATB have yet to be tested in flight. It is reasonable to believe that even greater gains could be achieved with the hybrid material technology.

A natural follow-up of the activity could consist in the design of a fully composite HATB with the optimization of the viscoelastic layers to cover the full operational temperature range.

One key characteristic of viscoelastic materials is their mechanical properties' dependence on parameters such as frequency, temperature, strain rate etc.

The HATB can experience significant temperature variations depending on the outside air temperature and the flight condition; therefore a second or third viscoelastic sheet, optimized for different temperature or frequency, can be integrated into the design. These layers would remain essentially dormant until their design temperature is reached, as shown in Figure 33. The concept can be exploited to achieve high loss factors over a wide temperature / frequency range.

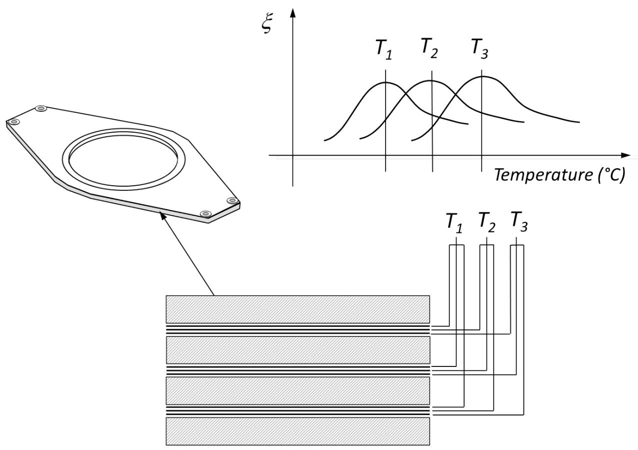

Figure 33: HATB viscoelastic layers optimized for multiple temperatures

It is noteworthy to observe that the HATB technology implies very little design trade-offs: has virtually no impact on the helicopter design, is easily retrofittable and potentially has very little weight penalty. Our HATB test item weighted a few kg more than the standard part, but this was due to the decision to keep the construction as simple as possible. It could easily be made lighter by replacing the aluminum closure plates with carbon fiber panels.

Future efforts will be focused on the design and test of optimised HATBs with the aim of reducing weight and increasing damping.

References

[1] B. C. Nakra. *Vibration Damping*. PINSA, 67, A, Nos. 4 - 5, pp. 461 478, July September 2001.

[2] Lumsdaine and R. A. Scott. *Shape Optimization of Unconstrained Viscoelastic Layers using Continuum Finite Elements*. Journal of Sound and Vibration, No. 216, pp. 29-52, 1998.

[3] V.K. Kinra and C.L. Yapura. *A Fundamental Connection Between Intrinsic Material Damping and Structural Damping*. M3D: Mechanics and Mechanisms of Material Damping, Vol. 1169, pp. 396-420, 1992.

[4] *MIL-HDBK-5J: Metallic Materials Elements for Aerospace Vehicle Structures*. DoD, 2003.

[5] *AMS-QQ-A-250/12: Aerospace material specification for aluminum alloy 7075*. SAE International, 2013.

[6] Luigi M. Bottasso, Gianluca Ghiringhelli, Alessandro Perazzolo, and Fausto Cenedese. *Helicopter with Noise and Vibration Damping Transmission Mounting*. Patent Grant EP 2962935 B1, 2014.

[7] A. Colombo, D. Ballerio, and S. Pancotti. *Helicopter*. Patent Grant EP 2179922, 2008.

[8] Jonas Oborn, Hans Bertilsson, and Mikael Rigdahl. *Styrene-Ethylene/Butylene-Styrene Blends for Improved Constrained-Layer Damping*. Journal of Applied Polymer Science, Vol. 80, issue 14, pp. 2865-2876, 2001.

[9] Conor D. Johnson and David A. Kienholz. *Finite Element Prediction of Damping in Structures with Constrained Viscoelastic Layers*. AIAA Journal, Vol. 20, No. 9, pp. 1284-1290, 1982.

[10] *ASTM E756-05: Standard Test Method for Measuring Vibration-Damping Properties of Materials*. ASTM International, 2010.

A APPENDIX

A.1 Structural damping principles

The damping characteristic of a viscoelastic material undergoing shear stress cycles can be described by the complex modulus G

(3) $$G = G_1 + iG_2 = G_1(1 + i\eta)$$

where $G = \sqrt{G_1^2 + G_2^2}$ represents the absolute value of the shear modulus and G_1, G_2 are its real and imaginary parts.

(4) $$\eta = G_2/G_1$$

is the $lossfactor$.

Stress and strain in purely elastic materials $(G_2 = 0)$ are always in phase; under these circumstances the response of strain to stress is immediate. In purely viscous materials $(G_1 = 0)$, strain lags stress by $90°$.

Viscoelastic materials exhibit an intermediate behavior, with some lag $(< 90°)$ in strain.

Viscoelastic materials can be modeled as a combination of elastic and viscous elements in series, in parallel or a mix of both; examples are shown in Figure 34.

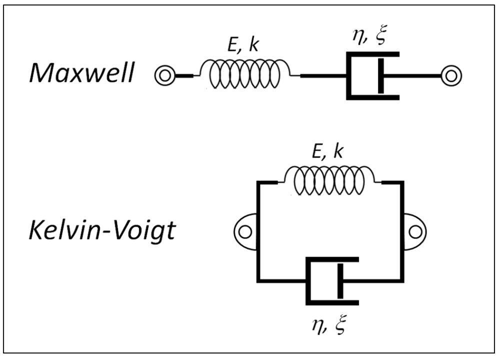

Figure 34: The Maxwell and Kelvin-Voigt viscoelastic material models

A.2 Noise metrics and effects on acoustic comfort

The sound pressure level (SPL) is a logarithmic measure of the mean squared pressure fluctuation of a sound relative to a reference value; it is measured in decibels (dB).

(5) $$SPL = 10\log_{10}\left(\frac{p_{rms}^2}{p_{ref}^2}\right) = 20\log_{10}\left(\frac{p_{rms}}{p_{ref}}\right)$$

The SPL measure is typically weighted to account for the relative loudness perceived by the human ear, whose sensitivity varies with sound frequency, reaching a maximum around 4 kHz. The most common weighing method is through the A-curve depicted in Figure 35, and is achieved by adding the curve values to the measured sound pressure levels in dB.

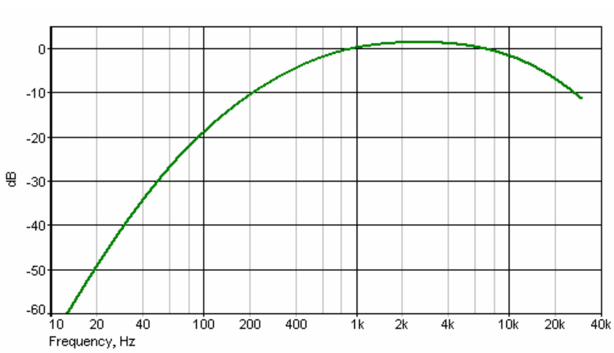

Figure 35: A-weighting curve

To facilitate comparison and analysis of acoustic measurements, normalized frequency bands have been standardised by ISO. There are two methodologies to subdivide the acoustic spectrum. In the traditional octave band approach the upper frequency of the band is twice the lower limit; the central frequency is defined as $f_c = \sqrt{2} f_{lower}$.

When more detailed spectral information is needed, the one-third octave band is used; in this case the upper and lower frequencies are linked by $f_{upper}/f_{lower} = \sqrt[3]{2}$ and the central frequency is $f_c = \sqrt[6]{2} f_{lower}$.

A notional A-weighted noise spectrum is depicted in Figure 36, where the peaks associated with the rotor blade passing frequencies and the drivetrain and clearly visible.

Another standard metric often used in helicopter acoustics is the SIL-4, or Speech Interference Level, computed as the arithmetic mean of the SPL measured on four one-third octave bands (central frequencies at 500 Hz, 1 kHz, 2 kHz, 4 kHz).

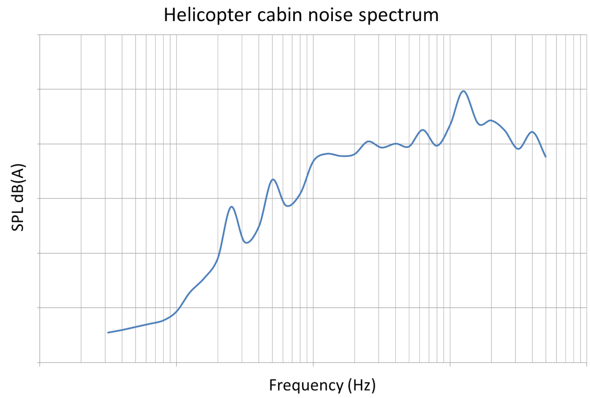

Figure 36: A typical noise spectrum as recorded inside a helicopter cabin